Arch Toxicol (2012) 86:483–496
DOI 10.1007/s00204-011-0772-4

ORGAN TOXICITY AND MECHANISMS

Pitavastatin, a new HMG-CoA reductase inhibitor, induces phototoxicity in human keratinocytes NCTC-2544 through the formation of benzophenanthridine-like photoproducts

Giampietro Viola · Pawel Grobelny · Maria Antonella Linardi · Alessia Salvador · Stefano Dall'Acqua · Łukasz Sobotta · Jadwiga Mielcarek · Francesco Dall'Acqua · Daniela Vedaldi · Giuseppe Basso

Received: 2 August 2011 / Accepted: 11 October 2011 / Published online: 29 October 2011

Abstract This study reports the results of an investigation of the phototoxicity mechanism induced by pitavastatin and its photoproducts, namely 6-cyclopropyl-10-fluoro-7,8-dihydrobenzo[*k*]phenanthridine (PP3) and 6-cyclopropyl-10-fluorobenzo[*k*]phenanthridine (PP4). The phototoxicity was tested in human keratinocytes cell lines NCTC-2544, and the results proved that under the same conditions, all three compounds exhibited phototoxic effects in the model tested. The reduction in cell viability was found to be both concentration- and UVA dose-dependent. A point of note is that both the photoproducts produced a dramatic decrease in cell viability with GI_{50} values one order of magnitude lower compared to the parent compound. In particular, the fully aromatic derivative (PP4) showed the highest antiproliferative activity. Flow cytometric analysis indicated that pitavastatin and the photoproduct PP4 principally induced necrosis, as revealed by the large appearance of propidium iodide-positive cells and also confirmed by the rapid drop in cellular ATP levels. Further studies committed to better understanding of photoinduced cell death mechanism(s) revealed that neither pitavastatin nor PP4 induced mitochondrial depolarization or lysosomal damage, but, interestingly, extensive cell lipid membrane peroxidation along with a significant oxidation of model proteins occurred, suggesting that pitavastatin and PP4 exert their phototoxic effect mainly in the cellular membranes. The present results suggest that the phototoxicity of pitavastatin may be mediated by the formation of benzophenanthridine-like photoproducts that appear to have high potential as photosensitizers.

Keywords Pitavastatin · Phototoxicity · Photoproduct · Necrosis · Lipid peroxidation · Protein oxidation

Abbreviations

BHA	2,6-di-tert-butylhydroxyanisole
BSA	Bovine serum albumin
DMTU	N–N′-dimethylthiourea
DNPH	2,4-dinitrophenylhydrazine
GSH	Glutathione reduced form
MDA	Malonyl dialdehyde
PIT	Pitavastatin
RNAse A	Ribonuclease A
SOD	Superoxide dismutase
TBA	Thiobarbituric acid
TOC	Tocopherol acetate

Introduction

Pitavastatin, NK-104, monocalcium bis(*3R*,*5S*,*6E*)-7-(2-cyclopropyl-4-[4-fluorophenyl]-3-quinolyl)-3,5-dihydroxy-

Electronic supplementary material The online version of this article (doi:10.1007/s00204-011-0772-4) contains supplementary material, which is available to authorized users.

G. Viola (✉) · M. A. Linardi · G. Basso
Department of Pediatrics, Laboratory of Oncohematology, University of Padova, Via Giustiniani 3, 35128 Padova, Italy
e-mail: giampietro.viola.1@unipd.it

P. Grobelny
Department of Pharmaceutical Technology, Poznan University of Medical Sciences, Grunwaldzka 6, 60-780 Poznań, Poland

A. Salvador · S. Dall'Acqua · F. Dall'Acqua · D. Vedaldi
Department of Pharmaceutical Sciences, University of Padova, via Marzolo 5, 35131 Padova, Italy

Ł. Sobotta · J. Mielcarek
Department of Inorganic and Analytical Chemistry, Poznan University of Medical Sciences, Grunwaldzka 6, 60-780 Poznań, Poland

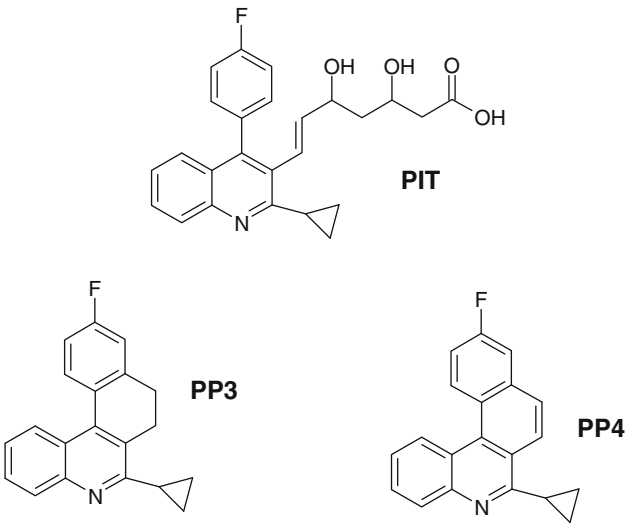

Fig. 1 Chemical structures of pitavastatin (PIT) and its main photoproducts PP3 and PP4

6-heptenoate (PIT, Fig. 1) is a totally synthetic HMG-CoA reductase inhibitor that significantly reduces serum total cholesterol, LDL cholesterol, and triglyceride levels while modestly raising HDL cholesterol (Kajinami et al. 2000, 2003). The cellular mechanism of action is attributed to the inhibition of cholesterol biosynthesis in the liver, and the drug is the first-line agent for lipid lowering in patients with atherosclerosis and cardiovascular disease (Ose et al. 2009). Additionally, recent reports have suggested that pitavastatin may exhibit pleiotropic effects and is now being tested for the treatment for other diseases, including Alzheimer's disease and osteoporosis (Mundy 2001; Caballero and Nahata 2004). Metabolism of pitavastatin by the cytochrome P450 system is minimal, principally through CYP 2C9, with little the involvement of the CYP 3A4 isoenzyme, potentially reducing the risk of drug–drug interactions (Fujino et al. 2003). Of great importance is a high systemic bioavailability resulting from a moderate first-pass metabolism, and the drug's long elimination half-life of approximately 11 h (Mukhtar et al. 2005).

Currently, the photostability of active pharmaceutical ingredients (APIs) as well as final dosage forms is of great interest because the photodegradation process can result in a loss of the potency of the drug and also in adverse effects due to the formation of toxic degradation products. It is accepted that fraction of the optical radiation above 300 nm can penetrate sufficiently deep into skin to react with substances circulating in the bloodstream. In case of new chemical entities for both topical and systemic application, which absorb light in the range of 290–700 nm, the phototoxic potential must be assessed through the use of appropriate assays. Thus, the study of the photostability of pharmaceuticals and their formulations is of more than simple scientific interest but has implications for the market.

The literature survey shows that certain statins including cerivastatin, atorvastatin, fluvastatin, and rosuvastatin are highly photochemically reactive (Krol et al. 1993; Cermola et al. 2006, 2007; Astarita et al. 2007). Moreover, we have recently concluded that the phototoxic potential of fluvastatin may be attributed to the formation of a polycyclic product with strong photosensitizing activity (Viola et al. 2010). The photodegradation of atorvastatin to a highly reactive phenanthrene-like photoproduct also may contribute to the phototoxic activity of the compound (Montanaro et al. 2009).

Our recent study (Grobelny et al. 2009) showed that pitavastatin exhibited susceptibility to degradation after exposure to UVA light, yielding polycyclic products. In particular, we noticed the formation of photoproducts after UVA exposure of the drug in aqueous media, indicating that photocyclization is the main reaction involved in the formation of the products observed. In this context, it would be of great importance to conduct experiments on the phototoxic potential of pitavastatin. Thus, the aim of this work is to evaluate the light-induced toxicity of pitavastatin and its main photoproducts in cultured NCTC-2544 human keratinocytes. In order to gain insight into the mechanism of phototoxicity, we have extended our studies to the photochemical damage on the protein model in vitro. To the best of our knowledge, this is the first report in which the phototoxic effects of pitavastatin are demonstrated at cellular level.

Experimental section

Chemicals

Pitavastatin calcium, monocalcium bis(3R,5S,6E)-7-(2-cyclopropyl-4-[4-fluorophenyl]3-quinolyl)-3,5-dihydroxy-6-heptenoate was obtained from Zydus Cadila, India.

Thiobarbituric acid (TBA), sodium azide (NaN_3), N–N′-dimethylthiourea (DMTU), superoxide dismutase (SOD), bovine serum albumin (BSA), ribonuclease A (RNAse A), 2,6-di-tert-butylhydroxyanisole (BHA), tocopherol acetate (TOC), and glutathione reduced form (GSH) were purchased from Sigma-Aldrich (Milano, Italy).

Irradiation procedure

Two HPW 125 Philips lamps, mainly emitting at 365 nm, were used for irradiation experiments. The spectral irradiance of the source was 4.0 mW cm^{-2} as measured at the sample level by a Cole-Parmer Instrument Company radiometer (Niles, IL, USA) equipped with a 365-CX sensor.

LC–MS analysis

Cells were irradiated in the presence of the compounds with different UVA doses, washed twice with Hank's Balanced Salt Solution (HBSS pH = 7.2), and then trypsinized and centrifuged. The resulting pellet was extracted with methanol, and the solution was subjected to LC–MS analysis. Varian 212 LC system equipped with a MS500 ion trap detector with ESI source was used for the HPLC–MS analysis. The MS conditions were the following: positive ion mode needle potential 5,400 V, shield 600 V, spray chamber temperature 50°C, nebulizer pressure 20 psi, drying gas pressure 18 psi, drying gas temperature 340°C, capillary voltage 78 V, RF loading 74%, MS range 50–700 Da. Parameters were optimized using the Varian WS workstation (optimizing by directly injecting 10 μL/min solution of pitavastatin). Agilent Eclipse plus C-18 (2.1 × 150 mm, 3.5 μm) was used as a stationary phase. Flow was 200 μL/min, and volume of injection was 5 μL. Eluents were water 0.1% HCOOH (A) and methanol (B), gradient elution was as follows: from 60% A to 0% A in 20 min, then isocratic at 0% A until 35 min.

Cellular phototoxicity

An immortalized, non-tumorigenic cell line of human keratinocytes (NCTC-2544) was grown in a DMEM medium (Sigma-Aldrich Milan, Italy), supplemented with 115 units/mL of penicillin G, 115 μg/mL streptomycin, and 10% fetal calf serum (Invitrogen, Milan, Italy). Individual wells of a 96-well tissue culture microtiter plate (Falcon, Becton–Dickinson) were inoculated with 100 μL of complete medium containing 8×10^3 NCTC-2544. The plates were incubated at 37°C in a humidified 5% CO_2 incubator for 18 h prior to the experiments. After medium removal, 100 μL of the drug solution, dissolved in DMSO and diluted with Hank's Balanced Salt Solution (HBSS pH = 7.2), was added to each well, incubated at 37°C for 30 min, and then irradiated. After irradiation, the solution was replaced with the medium and the plates were further incubated for 72 h. Cell viability was assayed by the MTT [(3-(4,5-dimethylthiazol-2-yl)-2,5 diphenyl tetrazolium bromide)] test as previously described (Viola et al. 2007).

Cellular localization studies

NCTC-2544 cells were allowed to attach in a sterile Petri dishes and treated with PIT or its photoproducts 100 and 20 μM, respectively, for 2 h, then washed with HBSS. Cellular fluorescence images were acquired with a video-confocal microscope (NIKON), using a Nir Apo 60×/1.0 W water immersion objective (Nikon Eclipse 80i, Melville, NY, USA).

Cell cycle analysis

For flow cytometric analysis of DNA content, 5×10^5 cells in exponential growth were irradiated as described above. After specified time intervals, the cells were trypsinized and together with floating cells, centrifuged, and fixed with ice-cold ethanol (70%). Subsequently, the keratinocytes were treated with a lysis buffer containing RNAse A and stained with propidium iodide. Samples were analyzed on a Beckman Coulter Cytomic FC500 flow cytometer. For cell cycle analysis, DNA histograms were analyzed using MultiCycle™ for Windows (Phoenix Flow Systems, CA, USA).

Externalization of phosphatidylserine

The surface exposure of phosphatidylserine (PS) by apoptotic cells was measured by flow cytometry with a Coulter Cytomics FC500 (Coulter) by adding Annexin-V-FITC to cells according to the manufacturer's instructions (Roche Diagnostic, Monza, Italy). Simultaneously, the cells were stained with PI. These experiments were performed in the presence or in the absence of different antioxidant added at the same time as PIT and the photoproduct.

Detection of DNA fragmentation by agarose gel

Total genomic DNA was extracted from irradiated keratinocytes by a commonly used salting out protocol. Afterward, 1 μg of DNA obtained was subsequently loaded on a 1.5% agarose gel at 50 V for 6 h in TAE buffer. After staining in an ethidium bromide solution, the gel was washed with water and the DNA bands were detected under UV radiation with an ImageQuant 300 transilluminator (GE Healthcare) equipped with a CCD camera.

Intracellular calcium measurement

The intracellular calcium concentration in NCTC-2544 cells was measured by flow cytometry using the Ca^{2+}-sensitive fluorescent dye Fluo-4/AM (Molecular Probes). Briefly, after specified time intervals, irradiated cells were washed and incubated with 2.5 μM Fluo-4/AM in the complete medium for 30 min at 37°C. The cells were then trypsinized, washed two times, and then resuspended in HBSS. The intracellular calcium level was analyzed immediately for Fluo-4/AM fluorescence intensity by flow cytometry.

ATP assay

Cells were irradiated in the presence of PIT or its photoproducts and from different times of irradiation, and the

cells were collected and counted. The ATP content per 100,000 cells was then determined using the CellTiter-Glo luminescent assay (Promega, Milano, Italy) according to the manufacturer's instructions, using a Victor^{3TM} luminometer (Perkin Elmer). Data are normalized to the ATP content in non-irradiated cells.

Caspase-3 assay

Caspase-3 activation in NCTC-2544 cells was evaluated by flow cytometry using a human active caspase-3 fragment antibody conjugated with FITC (BD Pharmingen). Briefly, after irradiation, the cells were collected by centrifugation and resuspended in Perm/Wash^{TM}(BD Pharmingen) buffer for 20 min, washed, and then incubated for 30 min with the antibody. After this period, the cells were washed and analyzed by flow cytometry.

Lipid peroxidation: TBARS assay

Lipid peroxidation was measured using a thiobarbituric acid assay as described previously (Viola et al. 2007). A standard curve of 1,1,3,3 tetraethxoypropane was used to quantify the amount of malonaldehyde produced. Data are expressed in terms of nanomoles of TBARS normalized to the total protein content, measured in an aliquot of the cell extract.

Protein oxidation

Solutions of bovine serum albumin (BSA) and ribonuclease A (RNAse A), (0.5 mg/mL) in the phosphate buffer 10 mM were irradiated in the presence of the test compounds for various times in a quartz cuvette. At different times, an aliquot of the solution was taken and the degree of protein oxidation was monitored spectrophotometrically, as described previously (Levine et al. 1990) by derivatization with 2,4-dinitrophenylhydrazine (DNPH).

Statistical analysis

Unless otherwise indicated, the results are presented as mean ± S.E.M. The differences between the irradiated and non-irradiated sample were analyzed using the two-sided Student's *t* test.

Results

Photolysis and cellular phototoxicity

Pitavastatin showed absorption maxima in the UVA range (320–400 nm) and underwent rapid photodegradation upon UVA irradiation in buffered aqueous solution, as previously reported (Grobelny et al. 2009). After irradiation, we were able to isolate by HPLC (Figure S1, see Supporting information) and characterize two main photoproducts that were subjected to NMR analyses. The isolated compounds were pure, as was determined by analytical HPLC and NMR analysis. NMR spectra (Table S1, see Supporting information) revealed structures consistent with tetracyclic compounds, namely 6-cyclopropyl-10-fluoro-7,8-dihydrobenzo[*k*]phenantridine (PP3) and (6-cyclopropyl-10-fluorobenzo[*k*]phenantridine (PP4) depicted in Fig. 1, in strong agreement with our previous results (Grobelny et al. 2009). Further experiments carried out with the purpose of evaluating the photostability of PP3 and PP4 evidently showed that the two photoproducts do not significantly modify their absorption spectra after UVA irradiation (Figure S2, Supporting information).

The phototoxicity of PIT and its photoproducts PP3 and PP4 was evaluated in a cell line of immortalized human keratinocytes NCTC-2544 by use of an MTT assay carried out 72 h after irradiation. Figure 2 (panel a) shows the reduction in viability obtained in NCTC-2544 cells at different concentrations and different UVA doses. As can be observed, a concentration and UVA dose-dependent reduction in cell viability is induced by PIT. The calculated GI_{50} is shown in Table 1. In the same experimental conditions, but in the absence of irradiation, PIT did not show any decrease in viability.

In the same model, the photoproducts PP3 and PP4 were tested. The two photoproducts did not affect cell viability without irradiation, but on the contrary, after irradiation, a reduction in cell viability can be observed for both compounds in comparison with the parent one, as showed in Fig. 2 (panels b, c). In particular, a remarkable decrease in cell viability was observed with the fully aromatic PP4 in comparison with the dihydro derivative PP3. Altogether, these data suggest that the phototoxicity of PIT could be mediated by the formation of these photoproducts.

UVA radiation induced photoproducts formation in NCTC-2544 keratinocytes

To evaluate whether PIT is converted to PP3 and/or PP4 in the cellular system, NCTC-2544 cells were irradiated in the presence of 100 μM PIT with the same UVA doses that induce cell killing and the cellular extracts were analyzed by LC–MS. As shown in Fig. 3 (panel a), after 2.5 J cm^{-2}, we were able to observe the appearance of two peaks corresponding to PP3 and PP4 indicating that the build up of the two photoproduct is effective also in a cellular system. Moreover, we analyzed the uptake of PIT and its photoproducts in NCTC-2544 cells utilizing their intrinsic fluorescence. As shown in Fig. 3 Panel b, we can observe

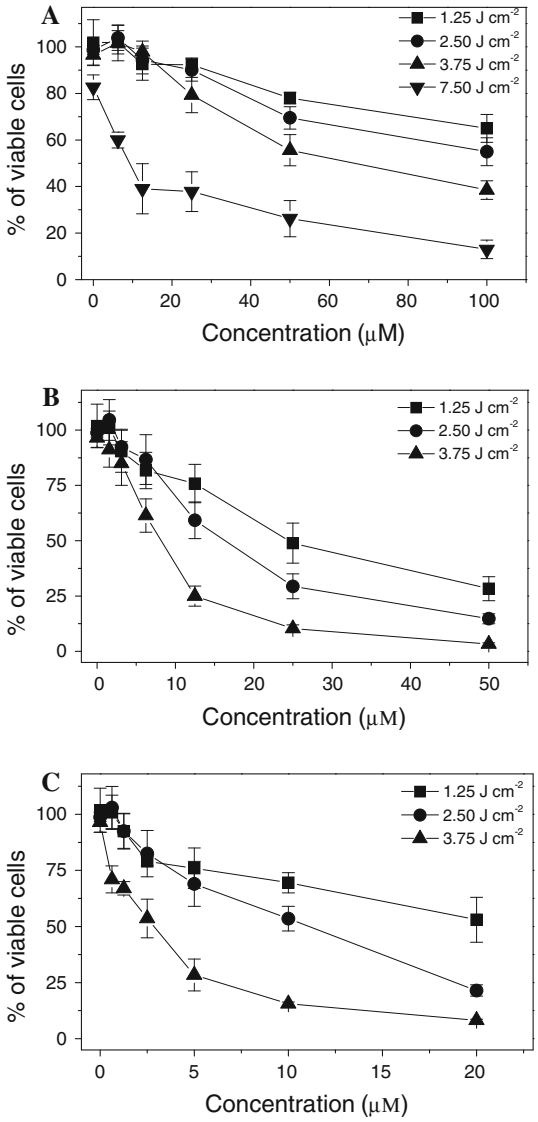

Fig. 2 Percentage of viability of human keratinocytes NCTC-2544 after UVA irradiation in the presence of PIT (panel **a**), photoproduct PP3 (panel **b**), and photoproduct PP4 (panel **c**). Cells were irradiated at the different UVA doses indicated and at different concentrations of compounds. Cell viability was measured by MTT test after 72 h after irradiation. Data represent mean ± S.E.M for at least four independent experiments

an efficient incorporation of the drugs inside the cells after 2 h of incubation without a particular disposition suggesting that both PIT and its photoproducts are able to bind and to penetrate inside the cells.

Assessment of the mode of cell death

To characterize the mode of cell death (necrosis or apoptosis) photoinduced by PIT and its most active photoproduct PP4, a biparametric cytofluorimetric analysis was performed in order to quantify the precise extent of

Table 1 GI_{50} of PIT, PP3, and PP4 after 72 h from the irradiation of NCTC-2544

UVA dose (J cm^{-2})	GI_{50}^{a}(μM)		
	PIT	PP3	PP4
1.25	>100	24.7	21.7
2.5	>100	16.4	11.1
3.75	78.1	8.2	2.8
7.5	8.7	n.d	n.d

[a] Drug concentration, expressed in μM, which reduces the cell proliferation by 50%

apoptosis versus necrosis using propidium iodide (PI) and Annexin-V (Martin et al. 1995). Positive staining with Annexin-V correlates with the loss of plasma membrane polarity but precedes the complete loss of membrane integrity that accompanies the later stages of cell death resulting from either apoptosis or necrosis. In contrast, PI can only enter cells after the loss of their membrane integrity. Thus, dual staining with Annexin-V and PI clearly allows to discriminate between unaffected cells (Annexin-V^-/PI^-), early apoptotic cells (Annexin-V^+/PI^-), late apoptotic cells (Annexin-V^+/PI^+), and necrotic cells (Annexin-V^-/PI^+).

Figure 4 shows six biparametric histograms as representative, in which the effect of PIT and PP4 at 24 and 48 h from the irradiation is depicted. It is quite evident that PIT and PP4 early induced an accumulation of PI-positive cells in comparison with the irradiated control.

A complete picture of the results is presented in Fig. 5 in which PIT and PP4 were used at the concentration of 100 and 20 μM, respectively. We did not observe a significant amount of A^+/PI^- cells at any time point investigated but, on the contrary, a large percentage of PI-positive cells was found, suggesting a rapid permeabilization of the cell plasma membrane that leads to necrotic cell death. Similar results were also obtained with lower concentrations of compounds (figure S3, Supporting informations).

The mode of cell death was also followed by two most common endpoint analyses, such as morphological changes and analysis of DNA fragmentation (Galluzzi et al. 2009). As shown in Fig. 6 (panel a), visual inspection by contrast-phase microscopy of the morphology of NCTC-2544 cells irradiated in the presence of PIT (100 μM) or PP4 (20 μM) revealed the presence of cellular swelling and rupture of the plasma membrane, which are typical signs of necrotic type of cell death. Furthermore, agarose gel electrophoresis of DNA extracted after 24 and 48 h from keratinocytes irradiated in the presence of PIT and PP4 (Fig. 6, panel b) showed a non-specific degradation resulting in a "smear" of randomly degraded DNA in the samples treated, which is indicative of necrotic cell death. In addition, to confirm the non-apoptotic cell death photoinduced by PIT and PP4,

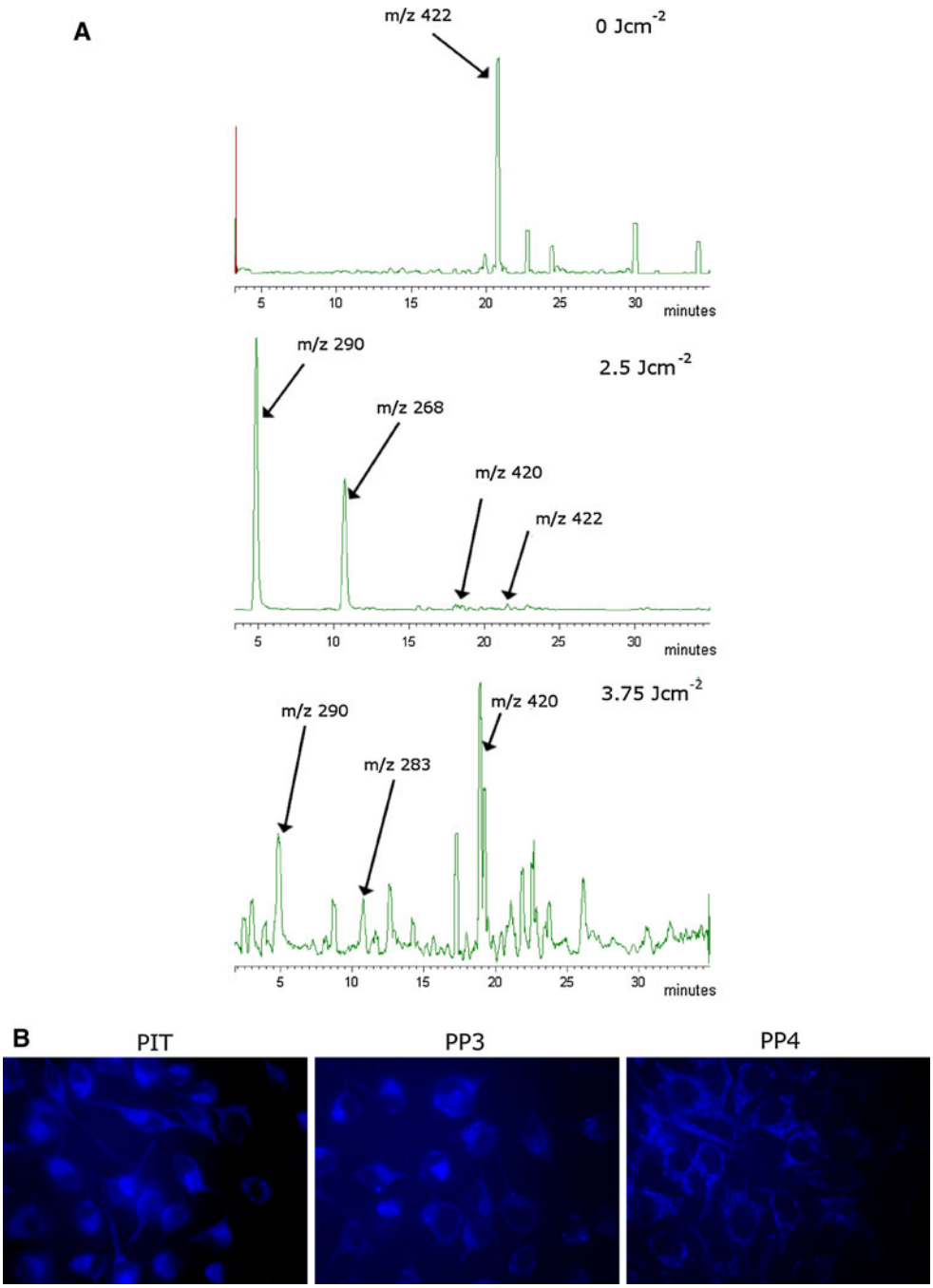

Fig. 3 Panel **a** LC–MS profile of NCTC cells after irradiation with PIT (100 μM) with the indicated UVA doses. Panel **b** Fluorescence microphotographs showing the intracellular localization of PIT, PP3, and PP4 in NCTC-2544 cells after 24 h of incubation at the concentration of 100 μM and 20 (PP3 and PP4), respectively

we evaluated the activity of caspase-3, since this enzyme is essential to the propagation of the apoptotic signal (Porter and Janicke 1999; Kumar 2007). As depicted in Fig. 6 (panel c), flow cytometric analysis of NCTC-2544 irradiated in the presence of PIT and PP4 did not show any activation of caspase-3.

Effect of antioxidant compounds

With the purpose of evaluating which reactive species are involved in the mechanism(s) of photoinduced cell toxicity, experiments irradiating NCTC-2544 cells with PIT and PP4 in the presence of different scavengers were performed, as previously reported (Elisei et al. 2004; Viola et al. 2007). The cell death was evaluated by flow cytometric analysis, by double staining of the cells with Annexin-V and PI. The additives used were NaN_3 (a singlet oxygen scavenger), superoxide dismutase (SOD, scavenger of $O^{\cdot -}$), DMTU (scavenger of $^{\cdot}OH$) and 2,6-di-tert-butylhydroxyanisole (BHA), tocopherol acetate, and GSH, (free radical scavengers). It can be observed from Fig. 7 that the photoinduced cell death by PIT and PP4 is

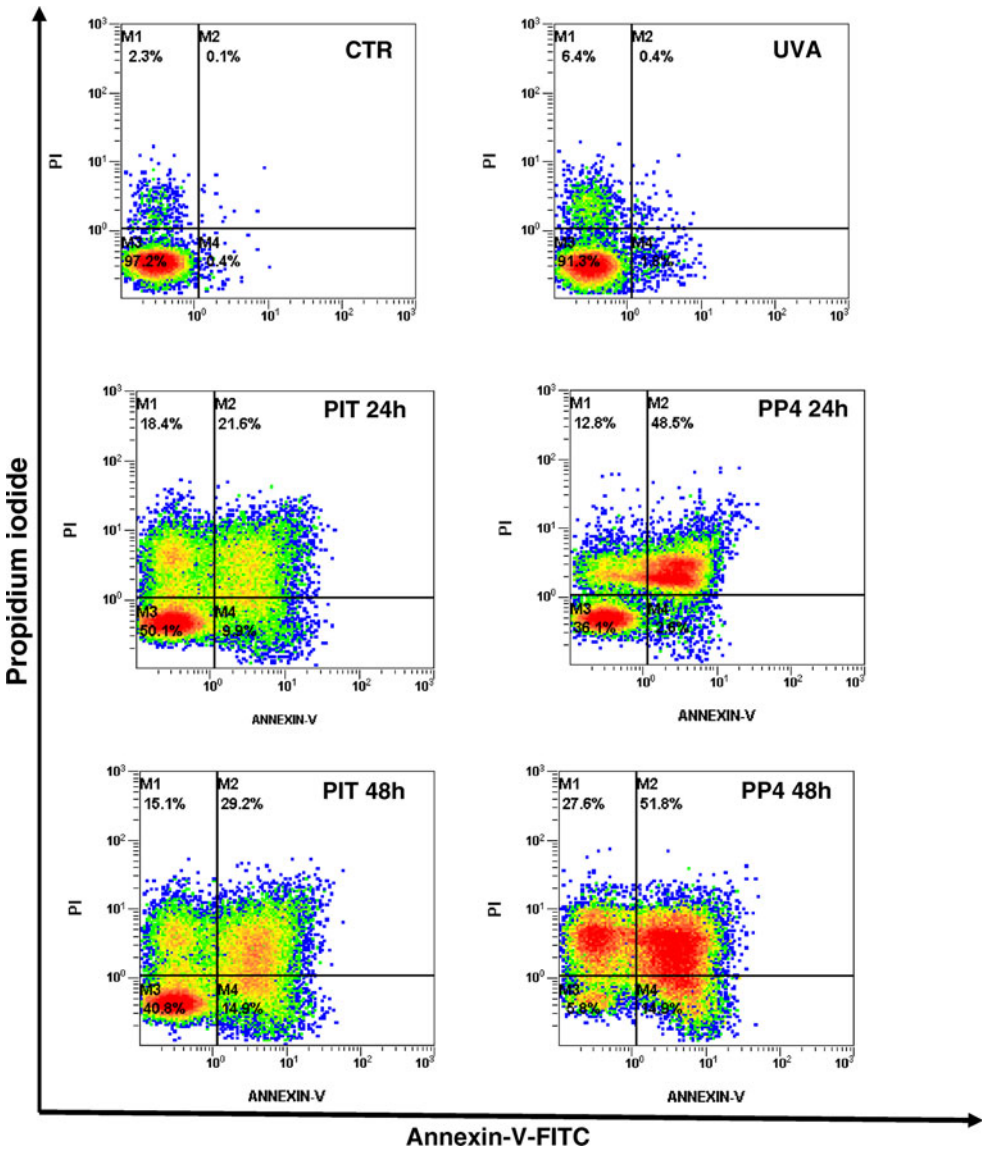

Fig. 4 Determination of the mode of cell death using Annexin-V and PI staining and flow cytometric analysis. Representative biparametric histograms obtained after 24 and 48 h after the irradiation (3.75 J cm^{-2}) of human keratinocytes NCTC-2544 in the presence of PIT 100 and PP4 20 μM

efficiently counteracted by GSH, BHA, and DMTU, which indicates that free and hydroxyl radicals may be involved in the mechanism of action.

ATP assay

Apoptosis is an energy-dependent process in which the decrease in ATP below critical levels may impede the execution of apoptosis and promote necrosis (Eguchi et al. 1997; Leist et al. 1997). In fact, necrosis is characterized by a rapid drop in ATP; given the potentially critical role attributed to ATP in the necrosis, we measured cellular ATP levels following irradiation with PIT and PP4. Using a luciferase-based assay for cellular ATP content, a dramatic depletion of ATP levels was detected in keratinocyte-irradiated cells in the presence of 100 μM PIT (Fig. 8). Similarly, the irradiation with 20 μM PP4 dramatically decreases ATP levels in comparison with non-irradiated cells; this was already seen after 12 h from irradiation, and a further reduction was detected at 24 h. Taken together, these data suggested that the rapid and pronounced ATP depletion was a concurrent event that accompanied the loss of cell viability.

Analysis of cell cycle

To investigate the effects of PIT and PP4 upon UVA irradiation on the cell cycle, NCTC-2544 cells were treated with the test compounds at different concentrations and at the light dose of 3.75 J cm^{-2}. After 12, 24, and 48 h from the irradiation, the cells were fixed and labelled with propidium iodide. The different phases of the cell cycle were analyzed by flow cytometry.

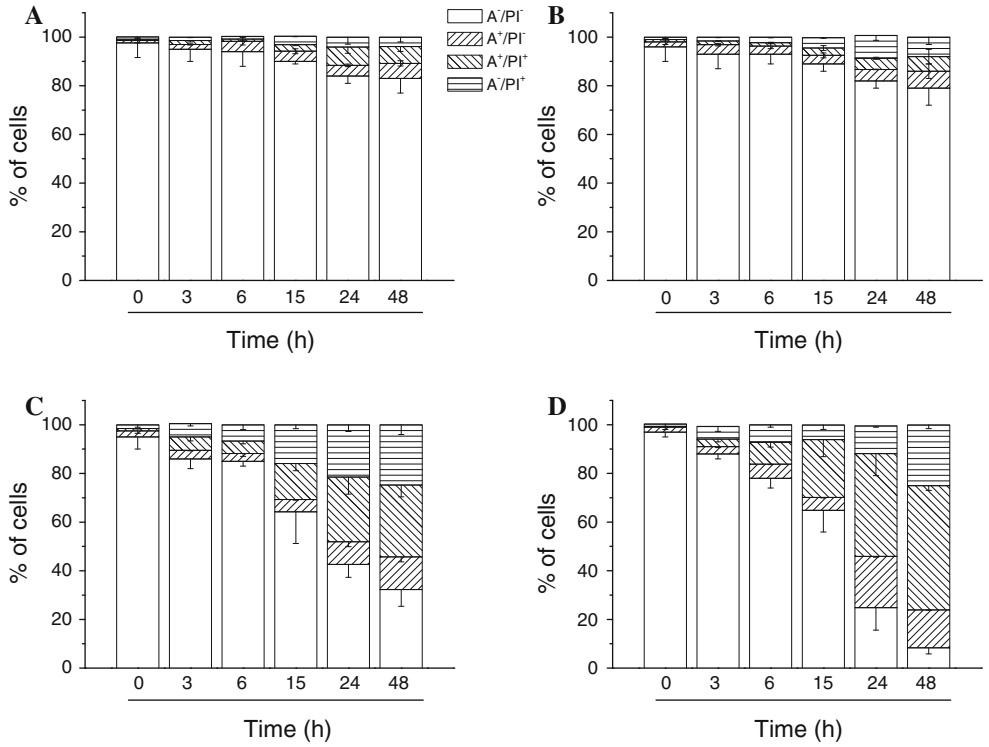

Fig. 5 Keratinocytes NCTC-2544 were irradiated in the presence of PIT at the concentration indicated, and after different times, the cells were collected, stained with Annexin-V-FITC and Propidium iodide (*PI*), and analyzed by flow cytometry. The results are expressed as a percentage of cells found in the different regions of the biparametric histograms showed in Fig. 4. Panel **a** Non-irradiated cells; Panel **b** UVA alone; Panel **c**: PIT 100 μM; Panel **d** 20 μM. Data represent the mean ± S.E.M of three independent experiments

Irradiation of keratinocytes with PIT induced an increase in the G2/M and S phase along with a reduction in the G1 phase (Table 2), in particular at 12 and 24 h after the treatment. On the contrary, after 24 h, PP4 induced an arrest of the cycle in the S phase. These data suggest that in response to phototoxic stress induced by the drugs, the progress of the cell cycle can be arrested at certain checkpoints that serve to maintain genomic integrity.

More importantly, it is interesting to note that the percentage of the cell population with a hypodiploid DNA content peak (subG1), representing those cells with a DNA content less than G1, which are usually considered as apoptotic cells, amounts to 10–20% at 24 h after treatment with PP4. Although statistically significant in respect to both control and UVA-treated cells, this represents a lower amount in comparison with the large percentage of dead cells (70%) as depicted in Fig. 5 and measured at the same time point.

Mitochondrial and lysosomal integrity assessment

To investigate which cellular sites are involved in the phototoxicity induced by PIT and the most active photoproduct PP4, we focused our attention on mitochondria and lysosomes. It has been shown previously that mitochondrial and/or lysosomal alterations are involved in cell death caused by many photosensitizers including fluoroquinolones, phenothiazines, antimalarial drugs, and porphyrins (Ouedraogo et al. 1999; Viola and Dall'Acqua 2006; Viola et al. 2007; Kessel and Luo 2001).

Further experiments to assess changes in mitochondrial functions after irradiation in the presence of PIT and PP4 were performed measuring the mitochondrial potential ($\Delta\psi_{mt}$) by flow cytometry. Flow cytometric analysis of NCTC-2544 cells after 24 or 48 h from the irradiation in the presence of the compounds showed no significant variations (Figure S4, Supporting information) of $\Delta\psi_{mt}$ in comparison with the irradiated control, indicating the non-involvement of this organelle in photoinduced cell death. To confirm that mitochondria were not involved in the photokilling mechanism, we also evaluated the mitochondrial production of ROS by two fluorescent probes, hydroethidine (HE) and 2′,7′-dichlorodihydrofluorescein diacetate (H_2DCFDA) by flow cytometry (Rothe and Valet 1990; Nohl et al. 2005). In agreement, only a slight increase in ROS production was observed for cells irradiated with PIT and PP4 (Figure S4, Supporting information).

In order to investigate the integrity of lysosomes after irradiation with the test compounds, flow cytometric

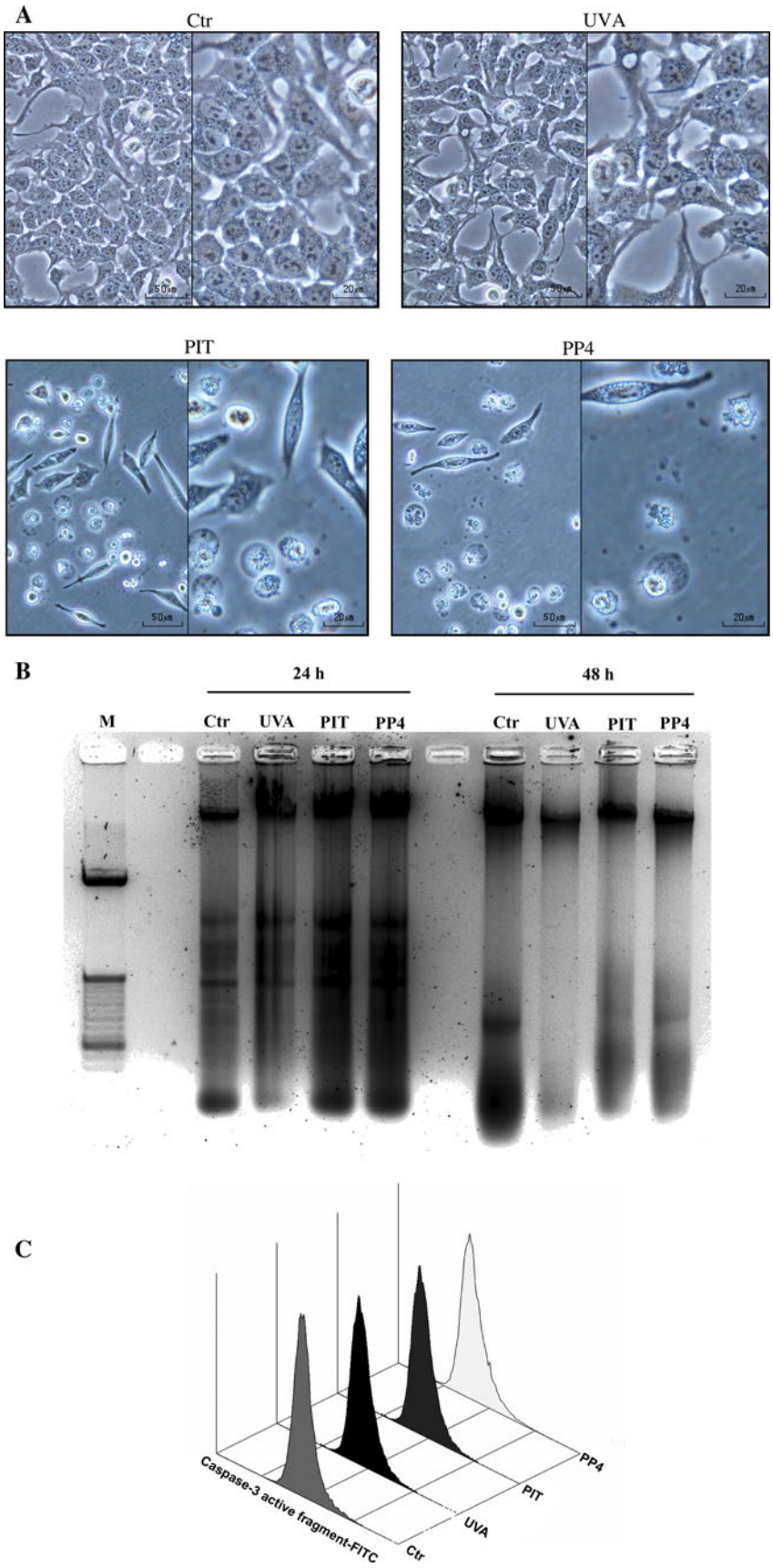

Fig. 6 Panel **a** Cell micrographs taken after 24 h from the irradiation (3.75 J cm^{-2}) in the presence of PIT and PP4 at the concentrations of 100 and 20 μM, respectively. Magnifications 20× and 40× Panel **b**. Agarose gel electrophoresis of chromosomal DNA extracted from NCTC-2544 cells 24 and 48 h after the irradiation (3.75 J cm^{-2}) in the presence of PIT (100 μM) and PP4 (20 μM). Lane *M* indicated size marker DNAs. Panel **c** Flow cytometric analysis of caspase-3 activity after irradiation in the presence of PIT (100 μM) and PP4 (20 μM). After 24 h of treatment, cells were harvested and stained with an antihuman active caspase-3 fragment monoclonal antibody conjugated with FITC. Representative histograms of three different experiments are shown

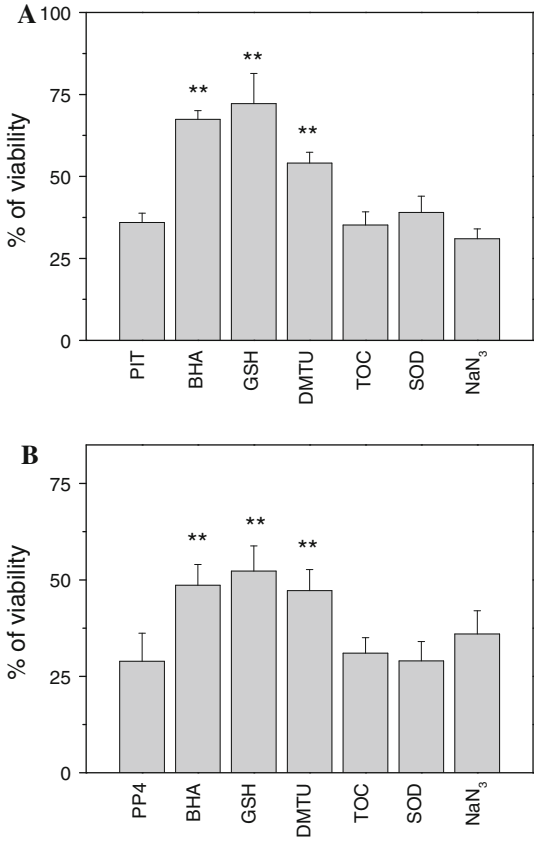

Fig. 7 Cell viability measured by flow cytometry by double staining of the cells with Annexin-V and PI, 24 h after irradiation in the presence of PIT 100 μM (panel **a**) and PP4 20 μM (panel **b**) and of BHA 10 μM, GSH 1 mM, DMTU 1 mM, SOD 2000 U.I., Tocopherol acetate (TOC) 200 μM and NaN_3 10 mM. Data represent the mean ± S.E.M of three independent experiments. $^{**}P < 0.01$ versus PIT or PP4 irradiated cells

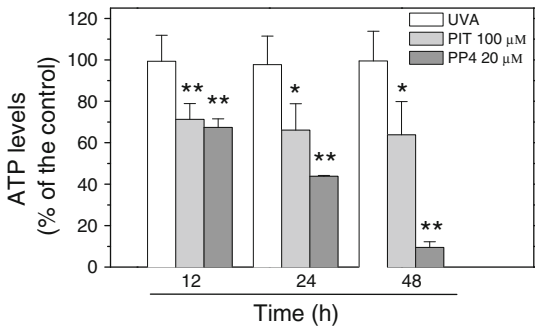

Fig. 8 ATP content was measured in NCTC-2544 cells after different times from the irradiation (3.75 J cm^{-2}) in the presence of PIT (100 μM) and PP4 (20 μM). Cells were collected and then counted, after which the ATP content per 100,000 cells was determined using the CellTiter-Glo luminescent assay (Promega, Milano, Italy) according to the manufacturer's instructions, using a Victor^{3TM} luminometer (Perkin Elmer). Data are normalized to ATP content in non-irradiated cells. Data represent the mean ± S.E.M of three independent experiments. $^{*}P < 0.05$, $^{**}P < 0.01$ versus UVA-irradiated cells

analysis was performed using the fluorescent acidotropic dye LysoTracker Red. The results (Figure S5, Supporting information) indicate only a slight reduction in fluorescence intensity, suggesting that lysosomes also do not represent a major target of the phototoxic action of the drugs.

Intracellular Ca^{2+} measurement

It has been demonstrated that the overload of intracellular Ca^{2+} is associated with the necrotic cell pathway (Golstein and Kroemer 2007). To verify whether a calcium signal is involved in the photoinduced cell death mechanism activated by PIT and PP4, we used the Ca^{2+}-sensitive dye Fluo-4/AM. The cells displayed an increase in Fluo-4/AM fluorescence intensity after just 1 h from irradiation, and the intensity was two–three times greater than the irradiated controls for both PIT and its photoproduct PP4 (Fig. 9, panels a, b).

To verify the source of calcium, we performed a similar experiment using a calcium-free medium containing 1 mM EGTA. The results showed (Fig. 9, panel c) that in these experimental conditions, a significant decrease in fluorescence occurred, indicating that the increased intracellular calcium is due to a calcium influx from the extracellular sites without calcium release from internal stores.

Lipid peroxidation

To gain insight into the photoinduced cell death mechanism activated by PIT and PP4, we investigated whether these compounds cause lipid peroxidation by measuring the level of malonyldialdehyde (MDA) bound to thiobarbituric acid (TBA) in treated and untreated NCTC-2544 cells. This assay is a measure of membrane injury as the cellular level of MDA correlates with lipid peroxidation (Girotti 2001). The results showed (Fig. 10), that in untreated cells or in UVA-irradiated cells, the levels of TBARS were relatively low. In contrast, the levels of TBARS increased significantly after 12 h after irradiation in the presence of PIT and PP4, and then, they further augmented at later times. Therefore, lipid peroxidation initiated by photoactivated PIT is well correlated with the increase in cell permeability measured with propidium iodide, suggesting that an extensive lipid peroxidation could play a major role in the photokilling mechanism.

Protein photodamage

To investigate more deeply the photosensitizing properties of PIT and PP4 toward other components of cellular membranes, such as proteins, aqueous-buffered solutions of PIT and PP4 containing bovine serum albumin (BSA) or

Table 2 Effect of PIT and PP4 on the cell cycle of NCTC-2544 after UVA irradiation (3.75 J cm^{-2})

	% G1[a]	% G2/M	% S	% Apoptotic Cells[b] (Sub-G1)
Ctr 12 h	65.1 ± 2.0	11.0 ± 1.9	25.6 ± 1.7	1.8 ± 0.1
UVA alone 12 h	64.6 ± 3.0	10.0 ± 1.7	25.4 ± 3.5	1.3 ± 0.2
PIT 12 h				
100 μM	37.3 ± 3.1*	25.6 ± 3.5*	37.1 ± 2.5	3.4 ± 1.5
50 μM	41.5 ± 6.0*	25.4 ± 1.0*	33.0 ± 7.1	2.2 ± 0.9
PP4 12 h				
20 μM	44.6 ± 2.8*	18.5 ± 1.5*	36.7 ± 4.1	4.2 ± 1.2
10 μM	33.7 ± 4.6*	29.1 ± 3.4*	37.2 ± 4.8	0.7 ± 0.1
Ctr 24 h	63.2 ± 3.4	11.6 ± 1.2	25.2 ± 2.8	1.0 ± 0.3
UVA alone 24 h	66.9 ± 3.5	14.1 ± 3.1	19.0 ± 1.5	5.4 ± 1.9
PIT 24 h				
100 μM	39.5 ± 5.1*	25.9 ± 3.1*	34.5 ± 8.1	2.2 ± 0.5
50 μM	45.5 ± 5.6*	21.9 ± 1.7*	32.6 ± 5.8	7.1 ± 2.2
PP4 24 h				
20 μM	43.5 ± 6.0	18.7 ± 1.9	43.6 ± 1.9*	24.8 ± 4.5*
10 μM	40.2 ± 5.5	19.3 ± 2.0	40.5 ± 7.5*	13.8 ± 1.4*
Ctr 48 h	62.8 ± 1.2	10.4 ± 2.9	26.8 ± 1.6	5.0 ± 1.5
UVA alone 48 h	63.4 ± 2.7	9.8 ± 0.5	26.6 ± 2.3	5.2 ± 1.0
PIT 48 h				
100 μM	58.2 ± 3.9	14.6 ± 2.0	27.3 ± 2.3	7.7 ± 1.4
50 μM	66.7 ± 3.2	17.6 ± 6.8	15.6 ± 3.5	9.5 ± 0.9
PP4 48 h				
20 Mm	53.5 ± 7.6	12.9 ± 3.7	33.6 ± 5.7	14.2 ± 3.2
10 μM	50.2 ± 6.6	19.6 ± 3.2	30.8 ± 6.2	11.6 ± 2.5

[a] The percentage of each phase of the cell cycle was calculated on living cells

[b] Percentage of the cell population with hypodiploid DNA content peak (apoptotic cells). Data expressed as the mean ± SEM of three experiments $*P < 0.05$ versus Ctr at the respective time

ribonuclease A (RNAse A) as models (Stadtman and Levine 2003) were irradiated for various times. The degree of oxidative modifications was measured by monitoring the carbonyl content, an index of oxidative damage of the proteins (Levine et al. 1990). RNAse A was selected as a protein model because of the lack of Trp residues, together with the presence of Tyr and Phe residues in its sequence. The results, reported in Fig. 11, demonstrated that PIT significantly increased the carbonyl content of BSA and RNAse A after irradiation, and this effect is both concentration- and UVA dose-dependent. On the contrary, PP4 only induced a slight increase in the carbonyl content for both BSA and RNAse A. This could be due to a lower binding of PP4 to the protein.

Discussion

As a continuation of our research into molecular mechanisms of the light-induced reactivity of drugs, we have examined the phototoxic effect of pitavastatin, a highly specific inhibitor of HMG-CoA reductase inhibitor. PIT fulfill the criteria for photosafety testing, including (1) high systemic bioavailability and long half-time; (2) administration over a long period of time; (3) degradation in solution during photoirradiation; (4) presence of essential chemical functionalities (aromatic moiety, double bond, fluorine atom); and (5) significant absorbance above 290 nm.

Pitavastatin, in combination with UVA light, induced a reduction in the cell viability, but more importantly, its photoproducts PP3 and PP4 showed a remarkable increase in the phototoxicity at a concentration ten times lower than the parent compound. It is interesting to note that the UVA doses used for the evaluation of phototoxicity are within the range of UVA doses sufficient to induce the photocyclization reaction resulting in efficient formation of photoproducts in vitro as demonstrated by LC–MS. Therefore, these results strongly suggest that the phototoxicity of PIT could be mediated by the formation of benzophenanthridine-like structures (PP3 and PP4) that act as strong photosensitizers.

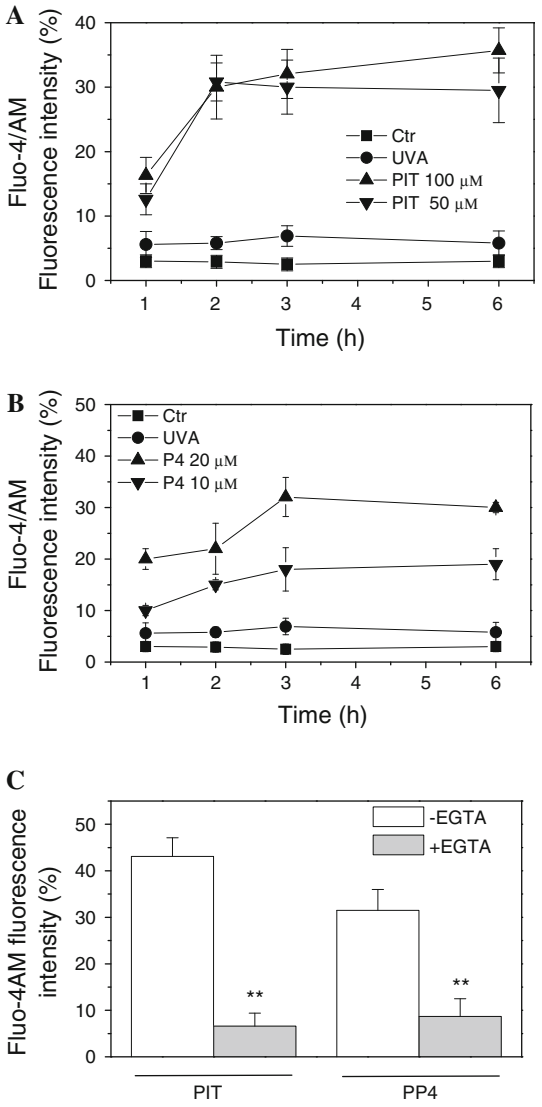

Fig. 9 Intracellular calcium measurement in NCTC-2544 cells after different times from the irradiation (3.75 J cm^{-2}) in the presence of PIT 100 and 50 μM (Panel **a**) and PP4 20 and 10 μM (Panel **b**). Ca^{2+} was measured by labeling the cells with 2.5 μM of Fluo-4/AM and examining the fluorescence by flow cytometry. Analogous experiments were performed in a calcium-free medium containing 1 mM EGTA (Panel **c**) and analyzed after 3 h from irradiation. Data represent the mean of fluorescence intensity ± S.E.M of four independent experiments. $^{**}P < 0.01$ versus UVA-irradiated cells

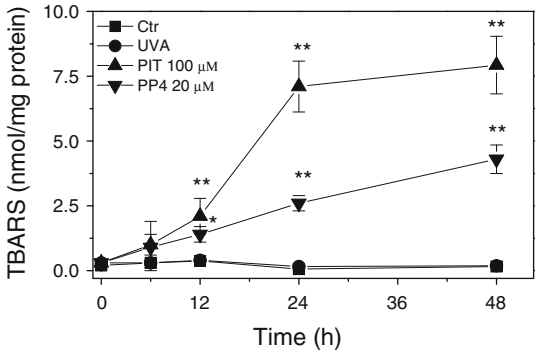

Fig. 10 TBARS assay in NCTC-2544 cells after different times from the irradiation (3.75 J cm^{-2}) with PIT and PP4 at the indicated concentrations. Data are expressed as the mean ± S.E.M. of three independent experiments. $^{*}P < 0.05$, $^{**}P < 0.01$ versus UVA-irradiated cells

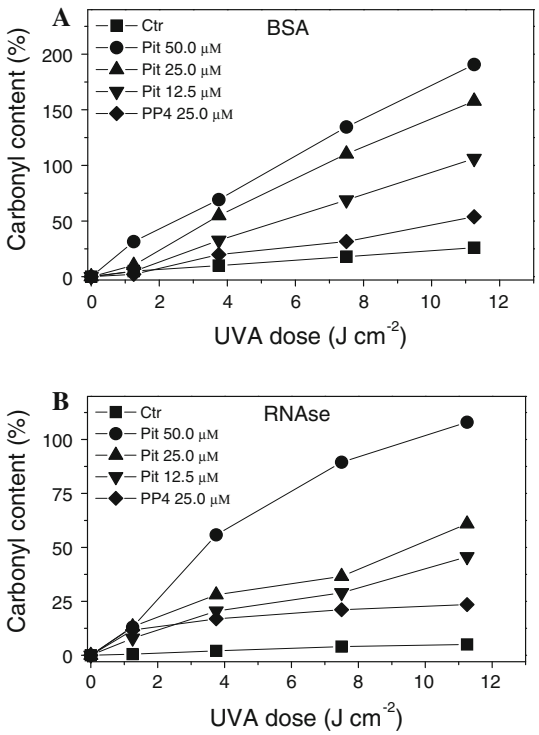

Fig. 11 Photosensitized protein oxidation by PIT and PP4. BSA (panel **a**), and RNAse A (panel **b**), dissolved in phosphate buffer 10 mM, pH = 7.2, were irradiated at different UVA doses in the presence of PIT and PP4 at the indicated concentrations. Protein oxidation was evaluated spectrophotometrically by monitoring the carbonyl content after derivatization with 2,4-dinitrophenylhydrazine (DNPH)

Soon after irradiation with PIT, cells initiated a series of remarkable morphological alterations that affect the integrity of the plasma membrane. In contrast, the nuclear structure is preserved and no DNA degradation is detected as also demonstrated by the analysis of DNA extracted from irradiated cells. These features are typical for necrotic cell death. Necrosis is associated with cell swelling, membrane rupture, and the release of cytosolic content to the external environment, whereby the loss of membrane integrity is considered an early event in this process.

In order to monitor the membrane integrity after irradiation with PIT, we used flow cytometry and double staining with Annexin-V and PI. Annexin-V staining precedes the loss of membrane integrity, which accompanies

the latest stages of cell death resulting from either apoptotic or necrotic processes. It should be noted that if the plasma membrane is permeabilized, Annexin-V can bind to intracellular phosphatidylserine as well (Galluzzi et al. 2009).

Our results showed a rapid increase in the PI-positive cells, whereas Annexin-V-positive cells did not increase significantly at any time investigated, suggesting that necrosis and not apoptosis is the major pathway of cell death. In excellent agreement with the MTT test, the photoproduct PP4 induced a high amount of PI-positive cells but at lower concentrations with respect to the parent compound indicating its involvement in the photoinduced cell death.

In this context, we observed a significant increase in intracellular Ca^{2+} concentration soon after the irradiation. Moreover, by depleting extracellular calcium with EGTA, we did not observe an increase in intracellular calcium after irradiation with PIT and PP4, which suggests that the increased intracellular Ca^{2+} was from extracellular sites and probably due to a rapid loss of membrane integrity resulting from lipid peroxidation as demonstrated by TBARS formation and protein oxidation.

The cell death induced by PIT and PP4 is accompanied by a reduction in the ATP content but not by the loss of mitochondrial membrane potential. Although the disruption of mitochondrial membrane potential plays an important role in necrotic and apoptotic processes, a lack of loss of mitochondrial membrane potential has been reported in non-apoptotic cell death (Kim et al. 2005). Given the rapid increase in cell membrane permeability after PIT or PP4 irradiation, as evidenced by intracellular Ca^{2+} increase and PI permeability, it is more plausible that these compounds cause considerable damage to the cell membrane structure, thereby promoting substantial ATP leakage into the extracellular spaces. As ATP depletion is considered to be the major cause of necrotic cell death, such a loss of the ATP pool may lead to necrosis. However, we cannot exclude the possibility that the drug may inhibit oxidative phosphorylation without any changes in mitochondrial membrane potential or that the reduction in ATP concentration could be due to an increase in ATP consumption.

Preliminary experiments devoted to evaluate which reactive species could be involved in the photoinduced cell death showed that the irradiation of keratinocytes in the presence of BHA, DMTU, and GSH significantly protects against cell death, indicating the involvement of free and/or hydroxyl radicals in the mechanism of action of both PIT and its photoproducts. Certainly, a detailed photophysical determination of the excited states generated after UVA absorption as well as reactive oxygen species is required for a better understanding of the mechanism of action.

In summary, we have established for the first time that PIT is endowed with a clear phototoxic potential in vitro in a human keratinocyte cell line. Its phototoxicity could be mediated by the formation of photoproducts endowed with high photosensitizing properties. Moreover, we identified plasma membrane as one of the major targets of the PIT action, which ultimately leads to necrosis as the principal mode of cell death. The photoproduct formation and the possible consequences on the biological effects of the photosensitization of cutaneous cells in patients treated with PIT deserve further studies.

Acknowledgments This work was supported by University of Padova and partially supported by Polish State Committee on Science (KBN, project No. NN405 3478 33).

References

Astarita M, Della Greca M, Iesce MR, Montanaro S, Previtera L, Temussi F (2007) Polycyclic compounds by sunlight exposure of the drug rosuvastatin in water. J Photochem Photobiol A 187:263–268

Caballero J, Nahata M (2004) Do statins slow down Alzheimer's disease? A review. J Clin Pharm Ther 29:209–213

Cermola F, Della Greca M, Iesce MR, Montanaro S, Previtera L, Temussi F (2006) Photochemical behavior of the drug atorvastatin in water. Tetrahedron 62:7390–7395

Cermola F, Della Greca M, Iesce MR, Montanaro S, Previtera L, Temussi F, Brigante M (2007) Irradiation of fluvastatin in water structure elucidation of photoproducts. J Photochem Photobiol A 189:264–271

Eguchi Y, Shimizu S, Tsuijmoto Y (1997) Intracellular ATP levels determine the cell death fate by apoptosis or necrosis. Cancer Res 57:1835–1840

Elisei F, Aloisi GG, Barbafina A, Dall'Acqua F, Mazzuccato U, Canton M, Facciolo L, Latterini L, Viola G (2004) Photophysical and photobiological behaviour of antimalarial drugs in aqueous solutions. Photochem Photobiol 79:248–258

Fujino H, Yamada I, Shimada S, Yoneda M, Kojima J (2003) Metabolic fate of pitavastatin, a new inhibitor of HMG-CoA reductase: human UDP-glucuronosyltransferase enzymes involved in lactonization. Xenobiotica 33:27–41

Galluzzi L, Aaronson SA, Abrams J, Alnemri ES, Andrews DW, Baehrecke EH, Bazan NG, Blagosklonny MV, Blomgren K, Borner C et al (2009) Guidelines for the use and interpretation of assays for monitoring cell death in higher eukaryotes. Cell Death Differ 16:1093–1107

Girotti AW (2001) Photosensitized oxidation of membrane lipids: reaction pathways, cytotoxic effects, and cytoprotective mechanisms. J Photochem Photobiol B 63:103–113

Golstein P, Kroemer G (2007) Cell death by necrosis: toward a molecular definition. Trends Biochem Sci 32:37–43

Grobelny P, Viola G, Vedaldi D, Dall'Acqua F, Gliszczynska-Swiglo A, Mielcarek J (2009) Photostability of pitavastatin—a novel HMG-CoA reductase inhibitor. J Pharm Biomed Anal 50:597–601

Kajinami K, Mabuchi H, Saito Y (2000) NK-104: a novel synthetic HMG-CoA reductase inhibitor. Expert Opin Investig Drugs 9:2653–2661

Kajinami K, Takekoshi N, Saito Y (2003) Pitavastatin: efficacy and safety profiles of a novel synthetic HMG-CoA reductase inhibitor. Cardiovasc Drug Rev 21:199–215

Kessel D, Luo Y (2001) Intracellular sites of photodamage as a factor in apoptotic cell death. J Porphyr Phthalocyanines 5:181–184

Kim WH, Choi CH, Kang S, Kwon CH, Kim YK (2005) Ceramide induces non-apoptotic cell death in human glioma cells. Neurochem Res 30:969–979

Krol GJ, Beck GW, Ritter W, Lettieri JT (1993) LC separation and induced fluorometric detection of rivastatin in blood plasma. J Pharm Biomed Anal 11:1269–1275

Kumar S (2007) Caspase function in programmed cell death. Cell Death Differ 14:32–43

Leist M, Single B, Castoldi AF, Kuhnle S, Nicotera P (1997) Intracellular adenosine triphosphate (ATP) concentration: a switch in the decision between apoptosis and necrosis. J Exp Med 185:1481–1486

Levine LR, Garland D, Oliver CN, Amici A, Climent I, Lenz AG, Ahn BG, Shaltiel S, Stadtman ER (1990) Determination of carbonyl content in oxidatively modified proteins. Methods Enzymol 186:464–480

Martin SJ, Reutelingsperger CP, McGahon AJ, Rader JA, van Schie RC, Laface DM, Green DR (1995) Early redistribution of plasma membrane phosphatidylserine is a general feature of apoptosis regardless of the initiating stimulus: Inhibition by overexpression of Bcl-2 and Abl. J Exp Med 182:1545–1556

Montanaro S, Lhiaubet-Vallet V, Iesce MR, Previtera L, Miranda MA (2009) A mechanistic study on the phototoxicity of atorvastatin: singlet oxygen generation by a phenanthrene-like photoproduct. Chem Res Toxicol 22:173–178

Mukhtar RY, Reid J, Reckless JP (2005) Pitavastatin. Int J Clin Pract 59:239–252

Mundy GR (2001) Statins and their potential for osteoporosis. Bone 29:495–497

Nohl H, Gille L, Staniek K (2005) Intracellular generation of reactive oxygen species by mitochondria. Biochem Pharmacol 69:719–723

Ose L, Budinski D, Hounslow N, Arneson V (2009) Comparison of pitavastatin with simvastatin in primary hypercholesterolaemia or combined dyslipidaemia. Curr Med Res Opin 25:2755–2764

Ouedraogo G, Morliere P, Bazin M, Santus R, Kratzer B, Miranda MA, Castell JV (1999) Lysosomes are sites of fluoroquinolone photosensitization in human skin fibroblasts: a microspectrofluorometric approach. Photochem Photobiol 70:123–129

Porter AG, Janicke RU (1999) Emerging role of caspase-3 in apoptosis. Cell Death Differ 6:99–104

Rothe G, Valet G (1990) Flow cytometric analysis of respiratory burst activity in phagocytes with hydroethidine and 2′, 7′-dichlorofluorescein. J Leukoc Biol 47:440–448

Stadtman ER, Levine RL (2003) Free radical-mediated oxidation of free amino acids and amino acid residues in proteins. Amino Acids 25:207–218

Viola G, Dall'Acqua F (2006) Photosensitization of biomolecules by phenothiazine derivatives. Curr Drug Targets 7:1135–1154

Viola G, Salvador A, Cecconet L, Basso G, Dall'Acqua F, Vedaldi D, Aloisi G, Elisei F, Latterini L, Barbafina A (2007) Photophysical properties and photobiological behaviour of amodiaquine, chloroquine and primaquine. Photochem Photobiol 83:1415–1427

Viola G, Grobelny P, Linardi MA, Salvador A, Basso G, Mielcarek J, Dall'Acqua S, Vedaldi D, Dall'Acqua F (2010) The phototoxicity of fluvastatin an HMG-CoA reductase inhibitor is mediated by the formation of a benzocarbazol-like photoproduct. Toxicol Sci 118:236–250